Dalton Transactions

Accepted Manuscript

ROYAL SOCIETY OF CHEMISTRY

www.rsc.org/dalton

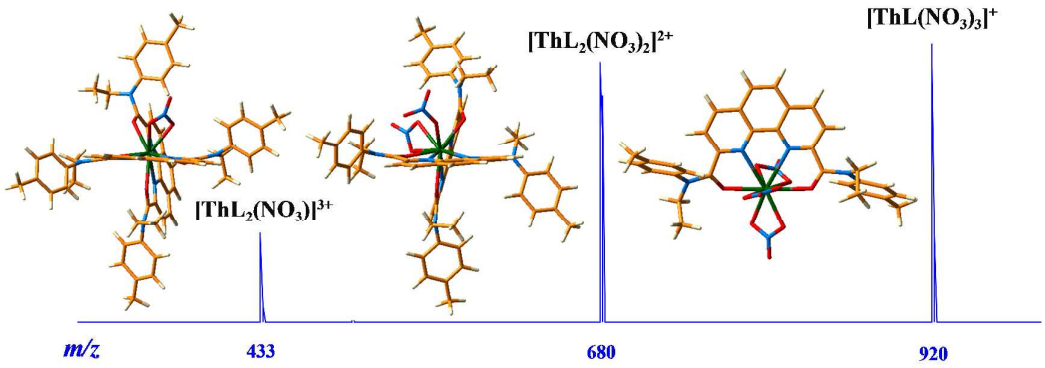

ESI-MS and density functional theory (DFT) methods were combined to understand the complexation mechanisms of tetradentate phenanthroline amide ligand with Eu(III), U(VI), and Th(IV) in acetonitrile solution.

Cite this: DOI: 10.1039/c0xx00000x

www.rsc.org/xxxxxx

ARTICLE TYPE

Europium, Uranyl, and Thorium-Phenanthroline Amide Complexes in Acetonitrile Solution: An ESI-MS and DFT Combined Investigation

Cheng-Liang Xiao,[a,b‡] Cong-Zhi Wang,[b‡] Lei Mei,[b] Xin-Rui Zhang,[b] Nathalie Wall,[c] Yu-Liang Zhao,[b] Zhi-Fang Chai,[a,b] and Wei-Qun Shi*[b]

Received (in XXX, XXX) Xth XXXXXXXXX 20XX, Accepted Xth XXXXXXXXX 20XX
DOI: 10.1039/b000000x

The tetradentate *N,N'*-diethyl-*N,N'*-ditolyl-2,9-diamide-1,10-phenanthroline (Et-Tol-DAPhen) ligand with hard-soft donor atoms has been demonstrated to be promising for the group separation of actinides from highly acidic nuclear wastes. To identify its formed complexes with actinides and lanthanides, electrospray ionization mass spectrometry (ESI-MS) combined with density functional theoretical (DFT) calculations was used to probe the possible complexation process. The 1:2 Eu-L species ($[EuL_2(NO_3)]^{2+}$) can be observed in ESI-MS at low metal-to-ligand ([M]/[L]) ratios whereas 1:1 Eu-L species ($[EuL(NO_3)_2]^{+}$) can be observed when the [M]/[L] ratio is higher than 1.0. However, ($[UO_2L(NO_3)]^{+}$) is the only detected species for uranyl complexes. The $[ThL_2(NO_3)_2]^{2+}$ species can be observed at low [M]/[L] ratio; the 1:2 species ($[ThL_2(NO_3)]^{3+}$) and a new 1:1 species ($[ThL(NO_3)_3]^{+}$) can be detected at high [M]/[L] ratios. Collision-induced dissociation (CID) results showed that Et-Tol-DAPhen ligands can coordinate strongly with metal ions and the coordination moieties remain intact under CID conditions. Natural bond orbital (NBO), molecular electrostatic potential (MEP), electron localization function (ELF), atoms in molecules (AIM) and molecular orbital (MO) analyses indicated that the metal-ligand bonds of actinide complexes exhibited more covalent characters than lanthanide complexes. Additionally, according to thermodynamic analysis, the stable cationic M-L complexes in acetonitrile are found to be in good agreement with the ESI-MS results.

Introduction

With the rapid development of nuclear energy, the reprocessing of spent nuclear fuel (SNF) is of great concern. Although the separation and recovery of U and Pu can considerably reduce the radiotoxicity of spent fuels, americium (Am) and curium (Cm) still remain in high level liquid wastes (HLLW) and account for the principal long-term radiotoxicity. The partitioning and transmutation (P&T) strategy[1-3] may provide a promising solution to largely minimize the radiotoxicity of headache nuclear wastes to the level of natural uranium. However, some lanthanides present in HLLW have high neutron absorption cross sections and can greatly decrease the transmutation efficiencies. Thus, actinides must be initially partitioned from lanthanides before transmutation. However, the separation of minor actinides (MA = Am, Cm) from lanthanides is quite challenging due to similar ionic radii and coordination modes of trivalent MA and lanthanides.[4]

In the past 15 years, considerable efforts have been made to develop novel and efficient extractants for the separation of MA(III) from Ln(III).[5-15] Extractants containing soft donors (e.g. sulfur or nitrogen) have been identified to possess better affinities for MA(III) than for Ln(III).[14,16-22] For example, extractants containing soft sulfur atoms (e.g. Cyanex 301) gained much attention in the past two decades, but the difficulty to completely incinerate them would result in the generation of secondary wastes.[16-19] According to the CHON principle (extractants containing only carbon, hydrogen, oxygen, and nitrogen elements), 2,6-bis(5,6-dialkyl-1,2,4-triazin-3-yl)pyridine (R-BTP),[20-23] 2,6-bis(5,6- dialkyl-1,2,4-triazin-3-yl)-2,2'-bipyridine (R-BTBP),[24-29] and 2,9-bis-(5,6-dialkyl-1,2,4- triazin-3-yl)-1,10-phenanthroline (R-BTPhen)[30-34] ligands have shown promising results for the separation of Ln(III)/MA(III). These heterocyclic extractants have been tested in the SANEX (Selective ActiNide EXtraction) process, in which R-BTPhen would be one of the most competitive ligand for MA(III)/Ln(III) separation in highly acidic wastes until now[34].

GANEX (Group ActiNide EXtraction) process[35-39] is another innovative concept, which aims at the recovery of most actinides (U, Np, Pu, Am, and Cm) from highly acidic liquid wastes. After the first cycle for the selective separation of uranium, transuranium elements in various oxidation states are simultaneously extracted using a multiple extractant system in the second cycle. The use of one single extractant instead of the combination of several ligands allows for simplication and separation efficiency. Miguirditchian et al[40, 41] have used a 6,6''-(2,2':6',2''-terpyridine)-diamide ligand for the group separation of actinides from lanthanides. Other similar ligands were designed by grafting amide or pyridyl-amide groups onto

phenanthroline skeleton.[42, 43] Unfortunately, the distribution ratios and selectivity of these ligands towards actinides were low in highly acidic solutions. Recently, our group has designed a tetradentate phenanthroline amide ligand that features a combination of hard-soft donors, *N*,*N'*-diethyl-*N*,*N'*-ditolyl- 2,9-diamide-1,10-phenanthroline (Et-Tol-DAPhen, Fig. 1).[44] Solvent extraction experiments showed that Et-Tol-DAPhen exhibited extremely high extractability and excellent selectivity for all actinides over metals even in the absence of any synergists. This ligand is one of the most efficient ligands for the group separation of actinides from fission products in highly acidic solution until now, which holds tremendous potential applications in the reprocessing of liquid nuclear wastes. However, the exact complex structures and complexation behaviours between this ligand and lanthanides as well as actinides still remain unclear.

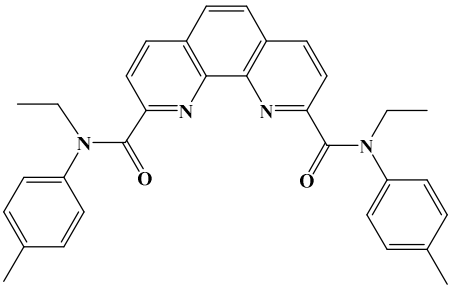

Fig. 1 Structures of *N*,*N'*-diethyl-*N*,*N'*-ditolyl-2,9-diamide-1,10-phenanthroline (Et-Tol- DAPhen, L).

Although the applications of ESI-MS for quantitative determination of existing species are somewhat controversial[45], this method is still efficient in identifying charged metal-ligand complexes in solution[46-51]. In the present work, ESI-MS was used to explore the chemical speciation of M-L (M = Eu, U, Th; L = Et-Tol-DAPhen) complexes in acetonitrile solution. In addition, the possible M-L complexes formed in acetonitrile solution were also studied using the density functional theory (DFT) calculation coupled with relativistic small-core pseudopotential. It is expected that this experimental and theoretical combined approach would provide insights for the understanding of the coordination modes and bonding nature between Et-Tol-DAPhen and the metals studied.

Experimental section

Reagents

The Et-Tol-DAPhen ligand was synthesized in our laboratory as reported previously.[44] Chemical reagents such as $Eu(NO_3)_3{\cdot}6H_2O$, $UO_2(NO_3)_2{\cdot}6H_2O$, and $Th(NO_3)_4{\cdot}5H_2O$ were of analytical grade. (Caution: *U and Th make radioactive hazards, which must be handled with care.*). Stock solution (5×10^{-4} M) of Et-Tol-DAPhen was prepared by dissolving a weighed amount in HPLC grade acetonitrile. Stock solutions (1×10^{-2} M) of Eu(III), U(VI), and Th(IV) were prepared by dissolution of corresponding nitrate salts in HPLC grade acetonitrile. All other chemicals were of analytical grade and were used without further purification.

ESI-MS Methods

Mass spectrometric measurements were recorded in positive ion mode using an amaZon SL ion trap mass spectrometer (Bruker Daltonics, Bremen, Germany) and an electrospray interface as ionization source. The nebulizer gas pressure was set to 8 psi and operating nitrogen at 5 L/min was employed as both the drying and nebulizing gas. The source temperature was set to 200 °C and the capillary voltage was 3500 V. Spectra were obtained over a mass range of m/z 200~1000. For MS/MS measurements, collision-induced dissociation (CID) of cluster ions was performed with helium. Samples were introduced using a 15 μL glass syringe with a stainless steel needle (Hamilton Co., Reno, NV, USA). Solutions for the ESI-MS measurements were prepared by mixing appropriate volumes of stock solutions of both ligand and metal nitrate in a 1.5 mL of plastic centrifuge tube. The ESI-MS spectra were measured at various metal-to-ligand ratios.

Theoretical Methods

Theoretical calculations were carried out using the density functional theory (DFT) method with the Gaussian 09 package[52]. The functional used is B3LYP, which combines Becke's three-parameter functional (B3)[53] with the Lee-Yang-Parr (LYP)[54] correlation functional. Relativistic effects were taken into consideration with the quasi-relativistic effective core potentials (RECPs)[55, 56]. The adopted small-core RECPs replace 60 core electrons for Th and U, and 28 electrons for Eu. The standard Pople-style polarized valence triple-ξ 6-311G(d, p) basis set was used for the C, H, O, and N atoms.

The structures of all the complexes were optimized in acetonitrile solution at the B3LYP/6-311G(d, p)/RECP level of theory with the conductor-like polarizable continuum model (CPCM)[57-60] with the Klamt atomic radii. The minimum energies of the optimized structures were checked by frequency analysis at the same level of theory. The natural atomic charges and Wiberg bond indices (WBIs)[61] were also calculated by natural bond orbital (NBO) analysis at the B3LYP/6-311G(d, p)/RECP level of theory. The enthalpy (H) and Gibbs free energy (G) were calculated including zero-point-energy (ZPE) and thermal corrections by the same method in acetonitrile solution. The electron localization function (ELF) and atoms in molecules (AIM) analyses were carried out with Multiwfn 3.2.1 package.[62] Additional details can be found in our previous studies[15, 26, 27, 63, 64].

Results and discussion

ESI-MS Results of Eu(III) Complexes

ESI-MS results of Eu-L complexes were recorded with a constant Et-Tol-DAPhen ligand concentration (5×10^{-4} M) at 25 °C. The experiments were carried out in the presence of Eu(III) with the metal-to-ligand concentration ratios ranging from 0 to 1.25. As shown in Fig. 2 and Table S1, the MS peak of the protonated Et-Tol-DAPhen ligand ($[L+H]^+$, m/z 503) is clearly observed in the absence of Eu(III). For the sample with metal-to-ligand ratio of 0.25, the intensity of the molecular ion peak of Et-Tol-DAPhen greatly decreases. Meanwhile, a new MS peak occurs at m/z 609, corresponding to the Eu(III) complex $[EuL_2(NO_3)]^{2+}$. With an increasing of [Eu(III)]/[L] ratio, the intensity of the ligand continues to decrease and the abundance of the MS peak at m/z 609 also increases. At a metal-to-ligand ratio of 1.0, the MS peak of the ligand almost disappears (0.44%) while a new Eu(III)

complex defined as $[EuL(NO_3)_2]^+$ at m/z 777 appears. At even higher metal-to-ligand ratio, the 1:2 complexes $[EuL_2(NO_3)]^{2+}$ is almost all dissociated and recombined into the 1:1 complexes. The compositions of all the Eu(III) complexes mentioned above were confirmed by the isotopic distributions in MS (Fig. S1).

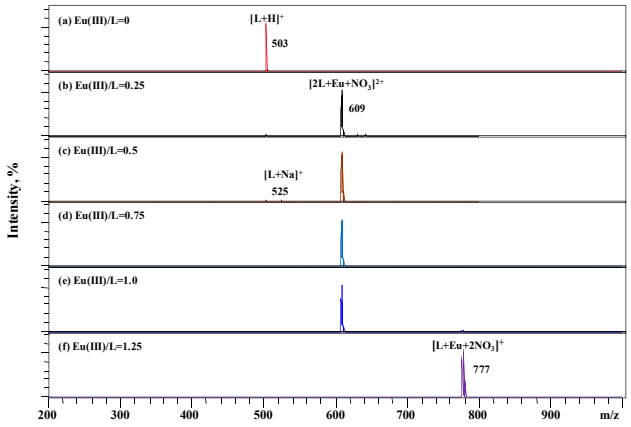

Fig. 2 ESI-MS of Eu(III) complexes at varous [Eu(III)]/[L] ratio.

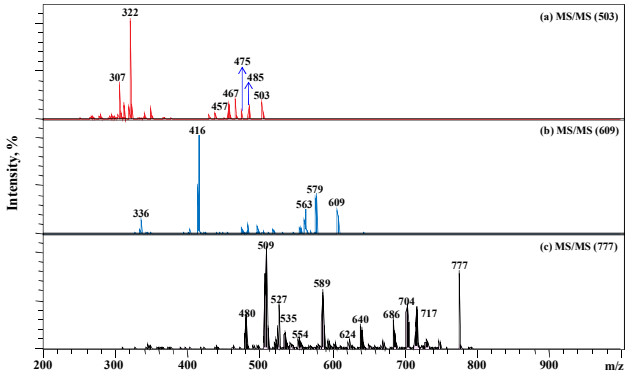

Fig. 3 MS/MS results of Eu(III) complexes.

To further investigate the coordination modes and stabilities of various complexes in MS, the CID technique was used to study the decomposition of parent ions. MS/MS results of molecular ion peaks at m/z 503, 609, and 777 are presented in Fig. 3 and Table S2. The fragments of the parent ion at m/z 503 mainly include MS peaks at m/z 485, 475, 467, 457, 322, and 307, corresponding to remaining species after elimination of -CH4-H_2, -C_2H_5+2H, -2CH_4-2H_2, -C_3H_7-H_2, -2C_7H_7+2H, and -2C_7H_7-CH_3+2H moieties, respectively. According to fragment analyses, it can be found that the side alkyl or aryl groups of amide moieties of the ligand readily decompose. Previous tandem mass spectrometric investigations showed that CID results can reveal decomposition behaviors similar to those of radiation-induced degradation to some extent, which could provide useful information for identifying radiolysis products[49, 50]. The MS/MS pattern of $[EuL_2(NO_3)]^{2+}$ at m/z 609 is presented in Fig. 3b. Similar to the Et-Tol-DAPhen ligand, the side amide moieties of $[EuL_2(NO_3)]^{2+}$ complex are also easily lost during the inert gas collision process. The species at m/z 579, 563, and 416 might correspond to the loss of two ethyl groups, one tolyl group, and four ethyl and three tolyl groups, respectively, from $[EuL_2(NO_3)]^{2+}$ complex. The MS peak at m/z 336 might stem from the elimination of one nitric acid molecule, four ethyl groups, and four tolyl groups from the $[EuL_2(NO_3)]^{2+}$ complex. For the $[EuL(NO_3)_2]^+$ complex at m/z 777 (Fig. 3c), the fragments still originate from the loss of side groups of amide moieties. The MS/MS peaks at m/z 717, 704, 686, 535, and 509 could be attributed to the elimination of two ethyl groups, two ethyl and one methyl groups, one tolyl group, two ethyl and two tolyl groups, and two N-ethyl-p-toluidine molecules from the $[EuL(NO_3)_2]^+$ complex, respectively, from the $[EuL(NO_3)_2]^+$ complex. Nevertheless, Et-Tol-DAPhen ligands can still coordinate strongly to the Eu(III) cations and neither one single ligand nor the Eu(III) cation are observed lost from intact or decomposed complexes during the CID experiments.

DFT Calculations of Eu(III) Complexes

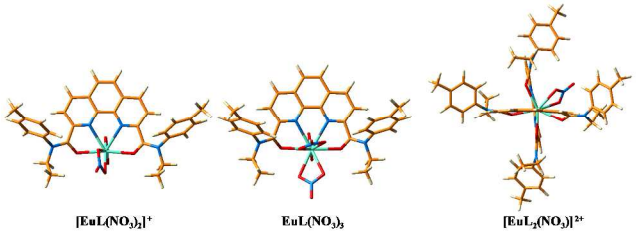

Fig. 4 Optimized structures of Eu(III) complexes in acetonitrile solution.

To explore the geometrical and electronic structures of the Eu(III) complexes, the molecular structures of the cationic species $[EuL(NO_3)_2]^+$ and $[EuL_2(NO_3)]^{2+}$ observed in the mass spectra have been optimized in acetonitrile solution at the B3LYP level (Fig. 4). Additionally, the molecular structure of neutral species $EuL(NO_3)_3$ is also optimized for comparison. For each species, Et-Tol-DAPhen coordinates with Eu(III) in a tetradentate mode through two nitrogen atoms of the phenanthroline moiety and two oxygen atoms of the amide moieties while nitrate anions are all bidentate ligands, forming 8- and 10-fold metal coordination (Fig. 4).

As listed in Table 1, the bond lengths of Eu-N and Eu-O in $[EuL(NO_3)_2]^+$ are shorter than those in $EuL(NO_3)_3$ and $[EuL_2(NO_3)]^{2+}$ due to the lower coordination number (CN=8) of $[EuL(NO_3)_2]^+$. For $EuL(NO_3)_3$ and $[EuL_2(NO_3)]^{2+}$ complexes with same coordination number (CN=10), the $[EuL_2(NO_3)]^{2+}$ exhibits longer Eu-N and Eu-O bond lengths, resulting from the steric effects of the Et-Tol-DAPhen ligands. It should be mentioned that, in each species, the Eu-O(L) bond lengths are shorter than the Eu-N(L) bond lengths by about 0.16 Å. This large bond length disparity suggests that amide oxygen atoms have relatively stronger electron-donating abilities toward Eu(III) compared to the phenanthroline nitrogen atoms. According to the NBO analysis, the WBIs of the Eu-N and Eu-O bonds for all the species are within the range of 0.24 to 0.34, indicative of small degree of covalent character of these bonds. As expected, Eu-O(L) bonds show higher WBIs values, which is in agreement with the results of the bond distances. Furthermore, based on the natural population analysis (NPA), the natural charges on the Eu atoms are much smaller than those of the free Eu^{3+} ion, suggesting important ligand-to-metal charge transfer in these species. Besides, the net charges of amide oxygen atoms are more negative than those of phenanthroline nitrogen atoms, which also confirm the stronger electron-donating abilities of the oxygen atoms.

Table 1 Average Eu-N and Eu-O Bond Distances (Å), Wiberg Bond Indices (WBIs) of Eu-N and Eu-O Bonds, and Natural Charges on the Eu, N, and O Atoms in the Eu(III) Complexes.

Complexes	Bond Length		Wiberg Bond Index		Natural Charge		
	Eu-N(L)	Eu-O(L)	Eu-N(L)	Eu-O(L)	Q_{Eu}	$Q_{N(L)}$	$Q_{O(L)}$
$[EuL(NO_3)_2]^+$	2.551	2.368	0.243	0.331	1.626	-0.492	-0.689
$EuL(NO_3)_3$	2.618	2.450	0.248	0.312	1.285	-0.456	-0.654
$[EuL_2(NO_3)]^{2+}$	2.629	2.462	0.251	0.310	1.338	-0.453	-0.645

In order to obtain more insight into the bonding nature of the Eu(III) complexes, the molecular electrostatic potential (MEP), electron localization function (ELF), and atoms in molecules (AIM) as well as molecular orbital (MO) analyses were also performed on the model complex of $[EuL(NO_3)_2]^+$.

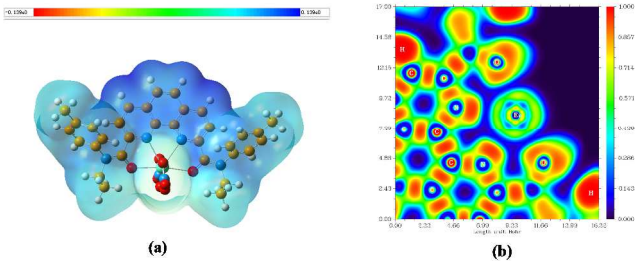

Fig. 5 (a) Molecular electrostatic potential surfaces (The isodensity contours are 0.0004 electron/bohr) and (b) two-dimensional (2D) plot of ELF for $[EuL(NO_3)_2]^+$.

According to the MEP analysis of $[EuL(NO_3)_2]^+$ (Fig. 5a), the region with relatively less positive charge is primarily concentrated over the oxygen and nitrogen atoms of the ligands, where there is a metal-ligand bonding. The ELF theory has been found to be a useful method for understanding electronic structures of compounds.[65-67] ELF values of 1 and 0 denote perfect localization and completely delocalized situation, respectively. Larger ELF values correspond to higher covalent character of chemical bonds. As shown in Fig. 5b, the ELF values of the Eu-N and Eu-O bonds are about 0.1, indicative of ionic character of these bonds.

In the AIM analysis, the electron density (ρ), the Laplacian of electron density ($\nabla^2\rho$), and the energy density (H(r)) at the bond critical points (BCPs), can be used to predict the bonding properties of complexes.[68, 69] Generally, $\rho > 0.20$ a.u. and $\nabla^2\rho < 0$ corresponds to a covalent bond or an open-shell interaction, while $\rho < 0.10$ a.u. and $\nabla^2\rho > 0$ indicates a closed-shell interaction (ionic, van der Waals, hydrogen, etc.). The magnitude of ρ can reflect the strength of chemical bonds. Furthermore, the negative H(r) value denotes covalent bonding, and positive H(r) value corresponds to closed-shell bonding. At the Eu-N and Eu-O BCPs in $[EuL(NO_3)_2]^+$, the small values of ρ and positive values of $\nabla^2\rho$ suggest the existence of electrostatic interactions in the Eu-N and Eu-O bonding. However, the slightly negative H(r) values of the Eu-N(L) and Eu-O(L) bonds suggest that these metal-ligand bonds may have some covalent characters.

Table 2 Average Electron Density (ρ), Laplacian ($\nabla^2\rho$), and Energy Density (H(r)) at Eu-N and Eu-O Bond Critical Points in $[EuL(NO_3)_2]^+$ (All values in a.u.).

Bonds	ρ	$\nabla^2\rho$	H(r)
Eu-N(L)	0.0431	0.1465	-0.0009
Eu-O(L)	0.0536	0.2302	-0.0001

To further investigate the covalent character of the metal-ligand bonding, some molecular orbitals (MOs) referring to the Eu-N and Eu-O bonding of the model complex $[EuL(NO_3)_2]^+$ are illustrated in Fig. 6. The occupied molecular orbitals displayed in Fig. 6a-6d and 6f correspond to the Eu-O(L) and Eu-O(NO_3^-) σ-bonding, respectively, which mainly results from 2p orbitals of the oxygen and nitrogen atoms and 5d, 4f orbitals of the europium atoms. The Eu-O(L), Eu-N(L) σ-bonding orbital (Fig. 6e) originates from the interactions of O, N 2p and Eu 4f orbitals.

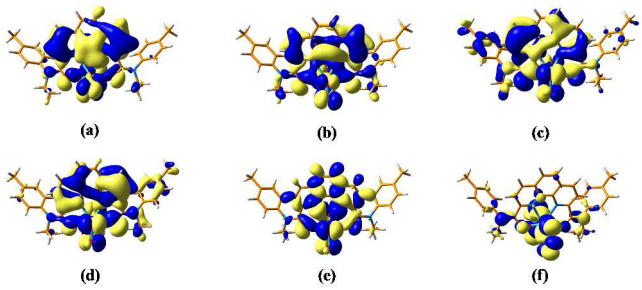

Fig. 6 Main molecular orbitals of $[EuL(NO_3)_2]^+$ referring to metal-ligand bonding.

Table 3 Changes in Enthalpy (Δ*H*), Entropy (*T*Δ*S*) and Gibbs Free Energy (Δ*G*) (kcal/mol) Including Zero-Point Energy (ZPE) and Thermal Corrections for the Complexation Reactions of Et-Tol-DAPhen and $[Eu(CH_3CN)_8]^{3+}$ or $[Eu(NO_3)(CH_3CN)_6]^{2+}$, $Eu(NO_3)_2(CH_3CN)_4]^+$, and $Eu(NO_3)_3(CH_3CN)_2$ in Acetonitrile Solution.

Reactions	Δ*H*	T*Δ*S*	Δ*G*
$[Eu(CH_3CN)_8]^{3+} + L + 2NO_3^- \rightarrow [EuL(NO_3)_2]^+ + 8CH_3CN$	-50.1	38.2	-88.2
$[Eu(CH_3CN)_8]^{3+} + L + 3NO_3^- \rightarrow EuL(NO_3)_3 + 8CH_3CN$	-71.6	26.3	-97.9
$[Eu(CH_3CN)_8]^{3+} + 2L + NO_3^- \rightarrow [EuL_2(NO_3)]^{2+} + 8CH_3CN$	-49.1	32.2	-81.3
$[Eu(NO_3)(CH_3CN)_6]^{2+} + L + NO_3^- \rightarrow [EuL(NO_3)_2]^+ + 6CH_3CN$	-32.8	28.4	-61.2
$[Eu(NO_3)(CH_3CN)_6]^{2+} + L + 2NO_3^- \rightarrow EuL(NO_3)_3 + 6CH_3CN$	-54.4	16.4	-70.9
$[Eu(NO_3)(CH_3CN)_6]^{2+} + 2L \rightarrow [EuL_2(NO_3)]^{2+} + 6CH_3CN$	-31.9	22.4	-54.2
$[Eu(NO_3)_2(CH_3CN)_4]^+ + L \rightarrow [EuL(NO_3)_2]^+ + 4CH_3CN$	-16.8	22.3	-39.1
$[Eu(NO_3)_2(CH_3CN)_4]^+ + L + NO_3^- \rightarrow EuL(NO_3)_3 + 4CH_3CN$	-38.3	10.4	-48.7
$[Eu(NO_3)_2(CH_3CN)_4]^+ + 2L \rightarrow [EuL_2(NO_3)]^{2+} + 4CH_3CN + NO_3^-$	-15.8	16.3	-32.1
$Eu(NO_3)_3(CH_3CN)_2 + L \rightarrow [EuL(NO_3)_2]^+ + 2CH_3CN + NO_3^-$	-5.5	12.9	-18.4
$Eu(NO_3)_3(CH_3CN)_2 + L \rightarrow EuL(NO_3)_3 + 2CH_3CN$	-27.1	1.0	-28.1
$Eu(NO_3)_3(CH_3CN)_2 + 2L \rightarrow [EuL_2(NO_3)]^{2+} + 2CH_3CN + 2NO_3^-$	-4.6	6.9	-11.4

Given that stock solution of Eu(III) was prepared by dissolution of corresponding nitrates in acetonitrile solution, we considered that the Eu(III) nitrates solvated with acetonitrile rather than the "free" metal ion as the substrate, i.e., Eu^{3+} ions, nitrate ions and CH_3CN may coexist in the substrate. To explore the possible species in acetonitrile solution, the complexes of $[Eu(CH_3CN)_8]^{3+}$, $[Eu(CH_3CN)_9]^{3+}$ and $[Eu(CH_3CN)_{10}]^{3+}$ were optimized at the same level, and our calculations (Table S5) show that the eight-coordinated complex is more favorable than the nine- and ten-coordinated species. Therefore, $[Eu(CH_3CN)_8]^{3+}$ was used as the reactant for the complexation reactions of Eu(III) with Et-Tol-DAPhen. In addition, the 8-fold-coordinated nitrate complexes with different number of bidentate nitrate ions in the first coordination sphere $[Eu(NO_3)(CH_3CN)_6]^{2+}$, $Eu(NO_3)_2(CH_3CN)_4]^{+}$, and $Eu(NO_3)_3(CH_3CN)_2$ were also considered in the complexing reactions. Table 3 shows the changes in enthalpy (ΔH), entropy (TΔS) and Gibbs free energy (ΔG) for these reactions. For all the reactions, the ΔH values are between -4.6 and -71.6 kcal/mol, and the TΔS values are all positive, resulting the ΔG values are in the range of -11.4 to -97.9 kcal/mol. This indicates that these reactions are exothermic in acetonitrile solution and these complexation processes can occur spontaneously at room temperature. For the reactions with $[Eu(NO_3)(CH_3CN)_6]^{2+}$, $Eu(NO_3)_2(CH_3CN)_4]^{+}$, and $Eu(NO_3)_3(CH_3CN)_2$ as reactants, the absolute values of ΔH, TΔS and ΔG are significantly smaller than those with $[Eu(CH_3CN)_8]^{3+}$. Hence, the reactions of $[Eu(CH_3CN)_8]^{3+}$ are preferable in acetonitrile solution. Besides, there are relatively large entropy contributions to the formation of $[EuL(NO_3)_2]^{+}$ and $[EuL_2(NO_3)]^{2+}$, but small entropy contributions for forming $EuL(NO_3)_3$. This indicates that the former reactions are mainly driven by entropy, while the latters are favorable in enthalpy. Compared with the absolute values of ΔG for all the reactions, the stabilities of these complexes follow the order of $EuL(NO_3)_3$ > $[EuL(NO_3)_2]^{+}$ > $[EuL_2(NO_3)]^{2+}$. Therefore, the two cationic complexes $[EuL(NO_3)_2]^{+}$ and $[EuL_2(NO_3)]^{2+}$ are the most probable ESI-MS species in positive ion mode.

ESI-MS Results of U(VI) Complexes

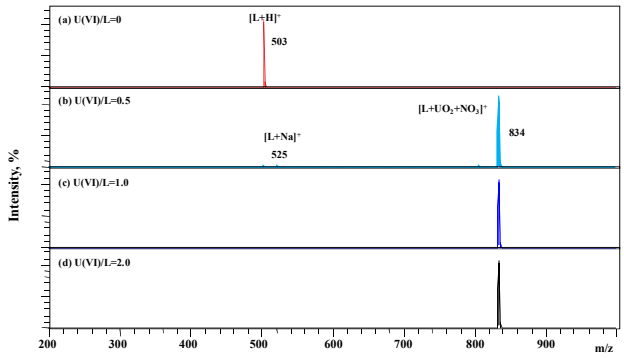

Fig. 7 ESI-MS results of U(VI) complexes at various [U(VI)]/[L] ratios.

ESI-MS measurements of U(VI) complexes were recorded after adding 0.01 M U(VI) into 1 mL of Et-Tol-DAPhen solution (5×10^{-4} M) in acetonitrile. The experiments were carried out with metal-to-ligand ratio varying from 0 to 2.0. As shown in Fig. 7 and Table S3, a ligand solution contacted with 0.25 equivalent of U(VI) leads to a significant decrease of the signal intensity of the protonated Et-Tol-DAPhen ligand ($[L+H]^{+}$, m/z 503). At the same time, a new U(VI) species identified as $[UO_2L(NO_3)]^{+}$ (Fig. S2) appears at m/z 834. Additionally, the MS peak at m/z 525 is attributed to the sodium ion adduct of the ligand ($[L+Na]^{+}$). With the increase of U(VI) concentration, the molecular ion peak of the ligand disappears gradually. When the [U(VI)]/[L] ratio is 1.0, the abundance of the protonated ligand is 0.45%. Furthermore, the molecular ion peak of the ligand disappears completely when the [U(VI)]/[L] ratio is 2.0. Correspondingly, only 1:1 U(VI) complex ($[UO_2L(NO_3)]^{+}$) is observed in MS whereas no other complexes with higher ligand-to-metal ratio are observed in this experimental conditions. The maximum coordination number of uranium is normally eight. For tetradentate Et-Tol-DAPhen ligand, it can provide four coordination sites. On account of two axial oxygen atoms in the uranyl ion, it is impossible for U(VI) to form the U(VI) complexes with high ligand-to-metal ratio.

The MS/MS results of $[UO_2L(NO_3)]^{+}$ complex at m/z 834 complex are displayed in Fig. 8 and Table S4. Similarly, the coordination of U(VI) with Et-Tol-DAPhen is so strong that fragments are eliminated only from the ligand molecules. The MS peaks at m/z 787, 774, 760, 742, and 641 in Fig. 8 might be attributed to the loss of $-2CH_4-CH_3$, $-2C_2H_6$, $-2C_2H_5-CH_4$, $-C_7H_8$, and $-2C_7H_7-CH_3$ fragments, respectively.

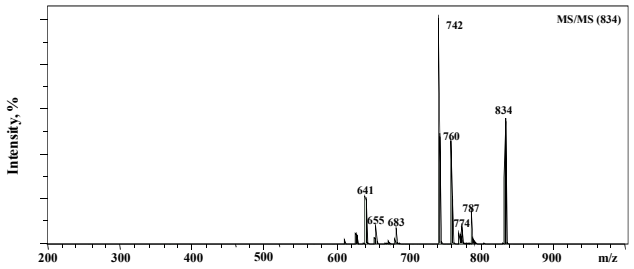

Fig. 8 MS/MS results of U(VI) complex.

DFT Calculations of U(VI) Complexes

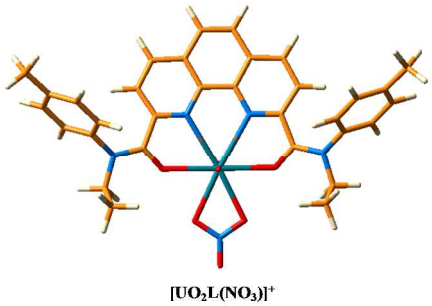

Fig. 9 Optimized structures of $[UO_2L(NO_3)]^{+}$ in acetonitrile solution.

As shown in Fig. 9, the structure of $[UO_2L(NO_3)]^{+}$ is optimized in acetonitrile solution at the B3LYP/6-311G(d,p)/RECP level of theory. Et-Tol-DAPhen and the nitrate anions are tetradentate and bidentate ligands, respectively, leading to six-membered chelate rings in the uranyl equatorial plane. U-N(L) bond lengths in $[UO_2L(NO_3)]^{+}$ are 2.644 Å (Table S6), which are much longer than those of U-O(L) bonds (2.417 Å). Accordingly, the WBIs of U-O bonds are slightly larger than those of U-N bonds and the amide oxygen atoms exhibit higher net charges, suggesting a larger donation from the amide oxygen atoms to uranium. In

addition, the small values for the WBIs of U-N and U-O bonds imply small covalent character of these bonding. It should be noted that since the geometrical structures of the U(VI) complexes we studied here were optimized in acetonitrile solution, the calculation results such as bond lengths and WBIs values from current work are different from those we reported previously[44], in which the corresponding structures were calculated in the gas phase. The metal net charge in $[UO_2L(NO_3)]^+$ (1.439) is significantly smaller than that in the free UO_2^{2+} cation (2.928), confirming significant ligand-to-metal donation in $[UO_2L(NO_3)]^+$ complex.

Table 4 Changes in Enthalpy (ΔH), Entropy ($T\Delta S$) and Gibbs Free Energy (ΔG) (kcal/mol) Including ZPE and Thermal Corrections for the Complexation Reactions of Et-Tol-DAPhen and $[UO_2(CH_3CN)_5]^{2+}$ or $[UO_2(NO_3)(CH_3CN)_3]^+$ and $UO_2(NO_3)_2(CH_3CN)$ in Acetonitrile Solution.

Reactions	ΔH	$T\Delta S$	ΔG
$[UO_2(CH_3CN)_5]^{2+} + L + NO_3^- \rightarrow [UO_2L(NO_3)]^+ + 5CH_3CN$	-45.0	21.5	-66.5
$[UO_2(NO_3)(CH_3CN)_3]^+ + L \rightarrow [UO_2L(NO_3)]^+ + 3CH_3CN$	-28.8	13.3	-42.1
$UO_2(NO_3)_2(CH_3CN) + L \rightarrow [UO_2L(NO_3)]^+ + CH_3CN + NO_3^-$	-16.5	5.7	-22.2

MEP analyses for $[UO_2L(NO_3)]^+$ (Fig. 10a) show that a relatively lower positive charged region is localized around the O and N atoms of the ligands. As shown in Fig. 10b, the U-N and U-O bonds are predominantly ionic according to the ELF analysis. On the basis of the AIM analysis (Table S7), the values of ρ are smaller than 0.1 a.u. and the $\nabla^2\rho$ values are about 0.2 a.u. indicating closed-shell interactions of the U-N and U-O bonds, while these bonds show negative H(r) values. Thus, the metal-ligand bonds may have partial covalent characters. Besides, some MOs contributing to the U-N and U-O bonding are shown in Fig. 11. The U-N(L) (Fig. 11a, b), U-O(L) (Fig. 11c, d) and U-O(NO_3^-) (Fig. 11e, f) σ-bonding orbitals mainly originate from 2p orbitals of N, O and 6d, 5f orbitals of U. Thermodynamic values for complexation reactions of U(VI) with Et-Tol-DAPhen were also calculated. Since the common coordination numbers are 5 and 6 in the uranyl equatorial plane, $[UO_2(CH_3CN)_5]^{2+}$ and $[UO_2(CH_3CN)_6]^{2+}$ were considered as the U(VI) solvated complexes in acetonitrile solution. As shown in Table S5, it was found that $[UO_2(CH_3CN)_5]^{2+}$ are more stable than $[UO_2(CH_3CN)_6]^{2+}$. This indicates that pentacoordination is more favorable for the uranyl ions in acetonitrile solution. Thus, the five-coordinated complex $[UO_2(CH_3CN)_5]^{2+}$ as well as the nitrate complex $UO_2(NO_3)_2(CH_3CN)$ were also considered in the complexation reactions of UO_2^{2+} with Et-Tol-DAPhen (Table 4). On the basis of reactions with $[UO_2(CH_3CN)_5]^{2+}$, $[UO_2(NO_3)(CH_3CN)_3]^+$, and $UO_2(NO_3)_2(CH_3CN)$ as reactants, the calculated ΔH, ΔG values are all negative and the TΔS values are all positve, indicating that these reactions are exothermic and can be spontaneous in acetonitrile solution at room temperature. Similar to the Eu(III) complexes, formation of $[UO_2L(NO_3)]^+$ with $[UO_2(CH_3CN)_5]^{2+}$ exhibits more negative ΔG values than those with $[UO_2(NO_3)(CH_3CN)_3]^+$ and $UO_2(NO_3)_2(CH_3CN)$, suggesting the preference of the former reaction in thermodynamics. Besides, the entropy contributions to the free energies of these reactions are relatively low.

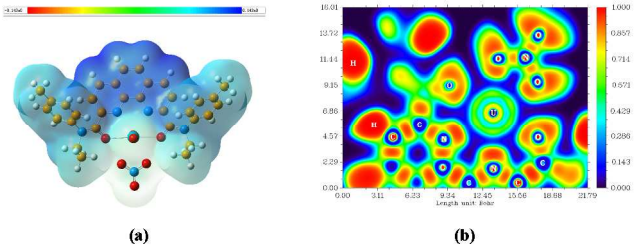

Fig. 10 (a) Molecular electrostatic potential surfaces (The isodensity contours are 0.0004 electron/bohr) and (b) two-dimensional (2D) plot of ELF for $[UO_2L(NO_3)]^+$.

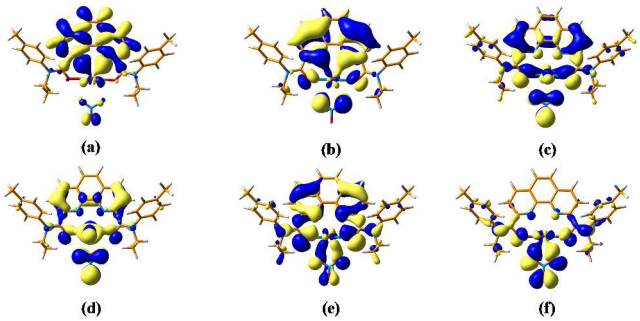

Fig. 11 Main molecular orbitals of $[UO_2L(NO_3)]^+$ referring to metal-ligand bonding.

ESI-MS Results of Th(IV) Complexes

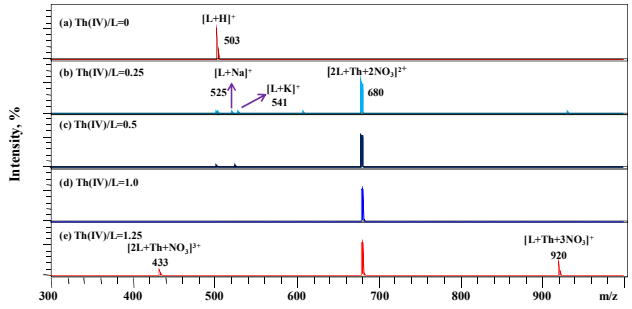

Fig. 12 ESI-MS results of Th(IV) complexes at various [Th(IV)]/[L] ratios.

Mass spectra of Th(IV) complexes were recorded with varying metal-to-ligand ratio from 0 to 2.0. As shown in Fig. 12 and Table S8, the MS of the protonated Et-Tol-DAPhen ligand ($[L+H]^+$, m/z 503) is reduced to 7.16% for a metal-to-ligand solution of 0.25. Meanwhile, a new MS peak at m/z 680 identified as $[ThL_2(NO_3)_2]^{2+}$ complex occurs. Two trace species at m/z 525 and 541 are attributed to $[L+Na]^+$ and $[L+K]^+$, respectively. With an increasing of metal-to-ligand ratio, the molecular ion peak of the ligand disappears gradually and the intensity of $[ThL_2(NO_3)_2]^{2+}$ species increases. At the metal-to-ligand ratio of 1.0, the MS peak of ligand is hardly observed. At higher Th(IV) concentration, two new MS peaks are observed at m/z 432 and 920, corresponding to $[ThL_2(NO_3)]^{3+}$ and $[ThL(NO_3)_3]^+$, respectively. Unlike the rapid disappearance of 1:2 Eu(III) species at higher metal-to-ligand ratios, the $[ThL_2(NO_3)_2]^{2+}$ species can still be observed even at the [Th(IV)]/[L] ratio of 2.0 (Table S5). The experimental isotopic distributions of all Th(IV) complexes identified in MS are quite

consistent with simulated ones (Fig. S3).

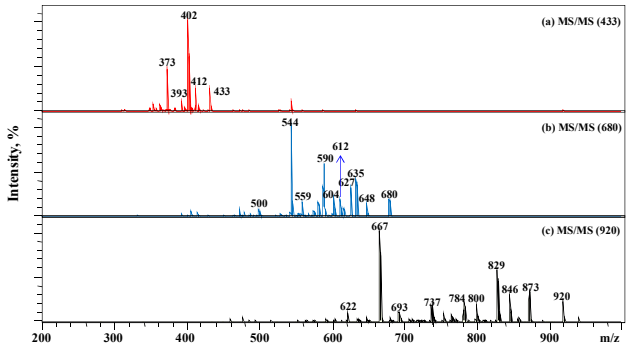

Fig. 13 MS/MS results of Th(IV) complexes.

MS/MS results of $[ThL_2(NO_3)]^{3+}$ (m/z 433), $[ThL_2(NO_3)_2]^{2+}$ (m/z 680), and $[ThL(NO_3)_3]^+$ (m/z 920) are presented in Fig. 13 and Table S9. The CID fragments of $[ThL_2(NO_3)]^{3+}$ (Fig. 9a) mainly include MS peaks at m/z 412, 402, and 373, which can be attributed to remnant fragments after loss of $-HNO_3$, $-HNO_3$-$2CH_3$+2H, and $-2C_7H_7$+2H moieties from $[ThL_2(NO_3)]^{3+}$ complex, respectively. Similarly, the peaks in the MS/MS pattern of $[ThL_2(NO_3)_2]^{2+}$ (Fig. 13b) might be due to the elimination of nitric acid molecule or the side groups of amide in the ligand, such as MS peaks at m/z 648 ($-HNO_3$), 635 ($-HNO_3$-$2CH_3$+2H), 612 ($-HNO_3$-$4CH_3$-CH_2), 590 ($-2C_7H_7$), and 544 ($-2C_7H_7$-$2C2H5$-$2CH_3$). Additionally, for $[ThL(NO_3)_3]^+$ complex (Fig. 13c), the fragments in the MS/MS are still resulted from the loss of side groups of the ligand. MS peaks at m/z 873, 846, 829, 800, 737, 667, and 622 might be attributed to the elimination of $-2CH_4$-CH_3, $-2C_2H_5$-CH_4, $-C_7H_7$, $-C_7H_7$-$2CH_3$+H, $-2C_7H_7$, $-2C_7H_7$-$2C_2H_5$-N, and $-2C_7H_7$-$2C_2H_5$-2NO from $[ThL(NO_3)_3]^+$ complex, respectively. In a word, the Et-Tol-DAPhen ligands bind Th(IV) ions so strongly that neither one single ligand molecule nor free Th(IV) ion is dissociated from the complexes. Only the side alkyl or aryl groups of amides in the ligand are eliminated during the CID experiments.

DFT Calculations of Th(IV) Complexes

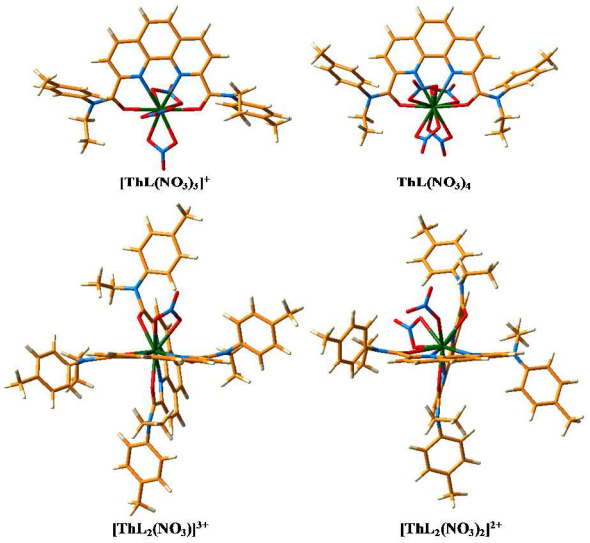

Fig. 14 Optimized structures of Th(IV) complexes in acetonitrile solution.

Four possible Th(IV) complexes including three cationic complexes observed in the mass spectrum and the neutral complex ThL(NO3)4 were optimized in acetonitrile solution at the B3LYP/6-311G(d,p)/RECP level of theory (Fig. 14). Similar to the Eu(III) and U(VI) complexes, the Et-Tol-DAPhen ligands are also coordinated as tetradentate ligands and most of the nitrate ions are bidentate ligands in these Th(IV) species, which results in 10- to 12-fold-coordinated complexes. As listed in Table 5, the Th-O(L) bond lengths are invariably significantly shorter than the corresponding Th-N(L) bonds. Th-O(L) bonds show larger WBIs values and the calculated natural charges of the amide oxygen atoms are higher compared to those of the phenanthroline nitrogen atoms. This confirms the relatively strong bonds between the thorium atoms and the amide oxygen atoms. Furthermore, the net charges on the Th atoms are much lower than that of free Th(IV) cations, giving another evidence of important charge transfer from the ligands toward the metal atoms.

Table 5 Average Th-N and Th-O Bond Distances (Å), Wiberg Bond Indices (WBIs), and Natural Charges on the Th, N, and O Atoms in the Th(IV) Complexes.

Complexes	Bond Length		Wiberg Bond Index		Natural Charge		
	Th-N(L)	Th-O(L)	Th-N(L)	Th-O(L)	Q_{Th}	$Q_{N(L)}$	$Q_{O(L)}$
$[ThL(NO_3)_3]^+$	2.663	2.404	0.315	0.461	1.581	-0.479	-0.672
$ThL(NO_3)_4$	2.711	2.474	0.329	0.454	1.044	-0.446	-0.629
$[ThL_2(NO_3)]^{3+}$	2.689	2.434	0.322	0.455	1.610	-0.464	-0.652
$[ThL_2(NO_3)_2]^{2+}$	2.790	2.476	0.314	0.450	1.298	-0.430	-0.630

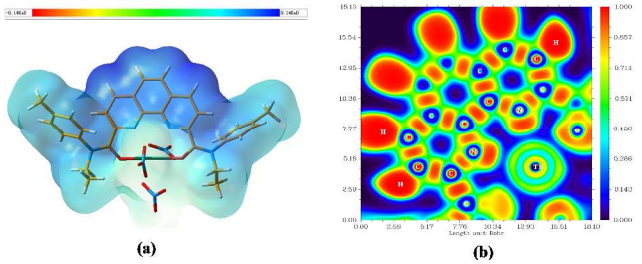

Fig. 15 (a) Molecular electrostatic potential surfaces (The isodensity contours are 0.0004 electron/bohr) and (b) two-dimensional (2D) plot of ELF for $[ThL(NO_3)_3]^+$.

Table 6 Average Electron Density (ρ), Laplacian ($\nabla^2\rho$), and Energy Density (H(r)) at Th-N and Th -O Bond Critical Points in $[ThL(NO_3)_3]^+$ (All values in a.u.).

Bonds	ρ	$\nabla^2\rho$	H(r)
Th-N(L)	0.0459	0.1119	-0.0039
Th-O(L)	0.0648	0.2137	-0.0063
Th-O(NO_3^-)	0.0496	0.1461	-0.0031

To explore the metal-ligand bonding nature of these complexes, the MEP, ELF, AIM and MO analyses have been carried out with $[ThL(NO_3)_3]^+$ as the model species. As it can be seen (Fig. 15), the O and N atoms of the ligands mainly exist in the region of relatively lower positive charge, and the small ELF values indicate the ionic bonding between the metal atoms and

the ligands. Although the values of ρ are smaller than 0.10 a.u. at the Th-N and Th-O BCPs and $\nabla^2\rho$ are all positive values, these bonds exhibit negative H(r) values (Table 6). Thus, it appears that the metal-ligand bonds have some degree of covalent character, which is similar to those of the Eu(III) and U(VI) species. According to the MO analysis (Fig. 16), the 2p nitrogen and oxygen orbitals and the 6d, 5f thorium orbitals mainly contribute to the Th-N and Th-O σ-bonding orbitals.

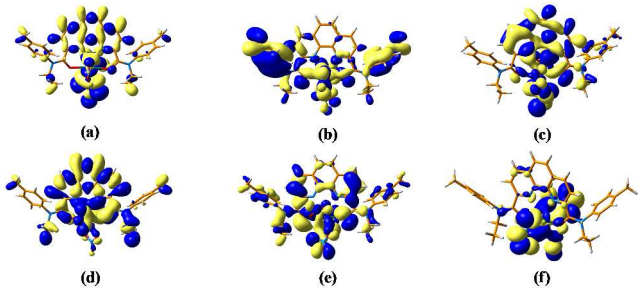

Fig. 16 Main molecular orbitals of $[ThL(NO_3)_3]^+$ referring to metal-ligand bonding.

Table 7 Changes of Enthalpy (Δ*H*) and Gibbs Free Energy (Δ*G*) (kcal/mol) Including ZPE and Thermal Corrections for the Complexation Reaction of Et-Tol-DAPhen and $[Th(CH_3CN)_9]^{4+}$ or $[Th(NO_3)(CH_3CN)_7]^{3+}$, $[Th(NO_3)_2(CH_3CN)_5]^{2+}$, $[Th(NO_3)_3(CH_3CN)_3]^+$ and $Th(NO_3)_4(CH_3CN)$ in acetonitrile solution.

Reactions	Δ*H*	TΔ*S*	Δ*G*
$[Th(CH_3CN)_9]^{4+} + L + 3NO_3^- \rightarrow [ThL(NO_3)_3]^+ + 9CH_3CN$	-93.3	37.9	-131.2
$[Th(CH_3CN)_9]^{4+} + L + 4NO_3^- \rightarrow ThL(NO_3)_4 + 9CH_3CN$	-114.7	23.1	-137.8
$[Th(CH_3CN)_9]^{4+} + 2L + NO_3^- \rightarrow [ThL_2(NO_3)]^{3+} + 9CH_3CN$	-71.4	43.0	-114.4
$[Th(CH_3CN)_9]^{4+} + 2L + 2NO_3^- \rightarrow [ThL_2(NO_3)_2]^{2+} + 9CH_3CN$	-87.1	33.4	-120.6
$[Th(NO_3)(CH_3CN)_7]^{3+} + L + 2NO_3^- \rightarrow [ThL(NO_3)_3]^+ + 7CH_3CN$	-71.0	30.2	-101.2
$[Th(NO_3)(CH_3CN)_7]^{3+} + L + 3NO_3^- \rightarrow ThL(NO_3)_4 + 7CH_3CN$	-92.5	15.4	-107.8
$[Th(NO_3)(CH_3CN)_7]^{3+} + 2L \rightarrow [ThL_2(NO_3)]^{3+} + 7CH_3CN$	-49.1	35.3	-84.4
$[Th(NO_3)(CH_3CN)_7]^{3+} + 2L + NO_3^- \rightarrow [ThL_2(NO_3)_2]^{2+} + 7CH_3CN$	-64.9	25.7	-90.6
$[Th(NO_3)_2(CH_3CN)_5]^{2+} + L + NO_3^- \rightarrow [ThL(NO_3)_3]^+ + 5CH_3CN$	-51.0	21.0	-72.0
$[Th(NO_3)_2(CH_3CN)_5]^{2+} + L + 2NO_3^- \rightarrow ThL(NO_3)_4 + 5CH_3CN$	-72.4	6.2	-78.6
$[Th(NO_3)_2(CH_3CN)_5]^{2+} + 2L \rightarrow [ThL_2(NO_3)]^{3+} + 5CH_3CN + NO_3^-$	-29.0	26.1	-55.2
$[Th(NO_3)_2(CH_3CN)_5]^{2+} + 2L \rightarrow [ThL_2(NO_3)_2]^{2+} + 5CH_3CN$	-44.8	16.6	-61.4
$[Th(NO_3)_3(CH_3CN)_3]^+ + L \rightarrow [ThL(NO_3)_3]^+ + 3CH_3CN$	-33.7	13.1	-46.7
$[Th(NO_3)_3(CH_3CN)_3]^+ + L + NO_3^- \rightarrow ThL(NO_3)_4 + 3CH_3CN$	-55.1	-1.8	-53.3
$[Th(NO_3)_3(CH_3CN)_3]^+ + 2L \rightarrow [ThL_2(NO_3)]^{3+} + 3CH_3CN + 2NO_3^-$	-11.8	18.1	-29.9
$[Th(NO_3)_3(CH_3CN)_3]^+ + 2L \rightarrow [ThL_2(NO_3)_2]^{2+} + 3CH_3CN + NO_3^-$	-27.5	8.6	-36.1
$Th(NO_3)_4(CH_3CN) + L \rightarrow [ThL(NO_3)_3]^+ + CH_3CN + NO_3^-$	-18.3	5.5	-23.8
$Th(NO_3)_4(CH_3CN) + L \rightarrow ThL(NO_3)_4 + CH_3CN$	-39.8	-9.3	-30.4
$Th(NO_3)_4(CH_3CN) + 2L \rightarrow [ThL_2(NO_3)]^{3+} + CH_3CN + 3NO_3^-$	3.6	10.6	-7.0
$Th(NO_3)_4(CH_3CN) + 2L \rightarrow [ThL_2(NO_3)_2]^{2+} + CH_3CN + 2NO_3^-$	-12.2	1.0	-13.2

The nine- to twelve-coordinated Th(IV) complexes were considered as the acetonitrile solvated species (Table S5), and the 9-fold-coordinated complex $[Th(CH_3CN)_9]^{3+}$ was found to be the most stable species (Table S5). To estimate the stability of the Th(IV) complexes with Et-Tol-DAPhen, the complexation reactions with the nine-coordinated species $[Th(CH_3CN)_9]^{3+}$ and $[Th(NO_3)(CH_3CN)_7]^{3+}$, $[Th(NO_3)_2(CH_3CN)_5]^{2+}$, $[Th(NO_3)_3(CH_3CN)_3]^+$, $Th(NO_3)_4(CH_3CN)$ as the reactants were investigated by the B3LYP method. As shown in Table 7, for the reactions with $[Th(CH_3CN)_9]^{3+}$ as reactant, the large negative ΔH and ΔG values indicate that these reactions are obviously exothermic and can occur spontaneously in acetonitrile solution. The absolute values of ΔH and ΔG significantly decrease with nitrate complexes $[Th(NO_3)(CH_3CN)_7]^{3+}$, $[Th(NO_3)_2(CH_3CN)_5]^{2+}$, $[Th(NO_3)_3(CH_3CN)_3]^+$, and $Th(NO_3)_4(CH_3CN)$ as reactants, especially for the formation of $[ThL_2(NO_3)]^{3+}$, in which the ΔH value is become positive with $Th(NO_3)_4(CH_3CN)$ as reactant. In addition to the reactions of $[Th(NO_3)_3(CH_3CN)_3]^+ + 2L \rightarrow [ThL_2(NO_3)]^{3+} + 3CH_3CN + 2NO_3^-$ and $Th(NO_3)_4(CH_3CN) + 2L \rightarrow [ThL_2(NO_3)]^{3+} + CH_3CN + 3NO_3^-$, all the reactions are predominantly driven by enthalpy. Besides, the neutral complex $ThL(NO_3)_4$ seems to be the most stable species according to the ΔH and ΔG values for all the reactions.

Comparison between ESI-MS and DFT Results

According to the above ESI-MS results, the complexation behaviors of Et-Tol-DAPhen ligand with Eu(III), U(VI), and Th(IV) have been disclosed. U(VI) forms only one $[UO_2L(NO_3)]^+$ complex, while Eu(III) and Th(IV) favor the formation of 1:1 complexes at higher [M]/[L] ratio and 1:2 complexes at lower [M]/[L] ratio with Et-Tol-DAPhen ligand. Furthermore, Th(IV) can form two 1:2 complexes, $[ThL_2(NO_3)_2]^{2+}$ and $[ThL_2(NO_3)]^{3+}$, depending on the [M]/[L] ratios added. It is worth mentioning that all the species detected by ESI-MS spectra contain nitrate anion, indicating that the nitrate anion is a strong ligand to bind with metal ion in a nitrate-rich media. Generally, the nitrate-coordinated species are dominant and bare positive species, such as $[UO_2L]^{2+}$, $[EuL]^{3+}$ and $[ThL_2]^{4+}$, are hardly formed under this condition. This result agrees well with those obtained from solvent extraction, single crystal structure, and optical spectrum for most tetradentate ligands[24-34]. With respect to forming different complexes with Et-Tol-DAPhen ligand for different actinide ions, it is probable due to the disparity of their oxidation states and coordination numbers. Compared to our previous results[44], this work demonstrates the formation of new 1:2 complexes for Eu(III) and Th(IV) with Et-Tol-DAPhen in addition to 1:1 complexes. This finding gives an indication that 1:2 complexes might be formed during the solvent extraction of Eu(III) and Th(IV) with Et-Tol-DAPhen, which is worth of further exploring.

What is more, we used DFT calculation to confirm the presence of species detected in ESI-MS spectra and further help to understand their chemical structures and bonding natures. For the thermodynamic analysis of the Eu(III), U(VI), and Th(IV) complexes, considering that the actinide nitrates were used for preparing corresponding stock solution in acetonitrile, the actinide cations may coexist with nitrate ions and CH_3CN in the substrate, and various complexing reactions with different complexes as reactants may take place in solution. Here, we mainly focus on two types of representative reactants with and without nitrate ions for the complexation reactions to explore the effects of CH_3CN and nitrate ions on the real reactions and probe

the possible complexation process. It should be noted that the coordination modes of nitrate ions might be versatile in actual reaction process, and different coordination modes of the nitrate ions would result in different thermodynamic values. In the present work, the inner-sphere coordination complexes are mainly considered as representatives, in which nitrate ions coordinated in bidentate fashion to metal cations for the thermodynamic analysis. According to our calculations, all the complexing reactions with $[Eu(CH_3CN)_8]^{3+}$, $[UO_2(CH_3CN)_5]^{2+}$, and $[Th(CH_3CN)_9]^{3+}$ as the reactants could be occurred spontaneously with negative enthalpy and positive entropy, and these reactions seem to be preferable in thermodynamics than those with nitrate complexes, e. g., $Eu(NO_3)_3(CH_3CN)_2$, $UO_2(NO_3)_2(CH_3CN)$, and $Th(NO_3)_4(CH_3CN)$. Besides, for reactions with nitrate complexes as reactants, the absolute values of ΔH and ΔG decrease with the number of nitrate ions increase. Therefore, we can deduce that the existence of CH_3CN in solution can promote the formation of Eu(III), U(VI), and Th(IV) complexes. Additionally, for all the complexing reactions, $[EuL(NO_3)_2]^+$, $[EuL_2(NO_3)]^{2+}$ and $[UO_2L(NO_3)]^+$ are the relatively stable cationic complexes for Eu(III) and U(VI), respectively. While for the Th(IV) complexes, $[ThL(NO_3)_3]^+$, $[ThL_2(NO_3)]^{3+}$, and $[ThL_2(NO_3)_2]^{2+}$ are predicted to be the possible cationic species. All these results are found to be in good agreement with the experimental data. For each of the Eu(III), U(VI) and Th(IV) complexes, the average M-O bond distances are found to be shorter than the M-N bonds, but the M-O bonds have higher WBIs values than M-N bonds. This indicates that the M-O bonds show higher covalent character compared to the M-N bonds, i.e., the amide oxygen atoms in Et-Tol-DAPhen ligand have stronger coordination ability to the metal ions. Additionally, the M-O and M-N bond in the U(VI) and Th(IV) species exhibit higher WBIs values than the Eu(III) species, suggesting higher covalent character of these bonds in the actinide complexes, which may be the main reason for the preference of the actinide ions with the Et-Tol-DAPhen ligand. For all the complexes, MO analysis confirms the covalent interaction of the metal-ligand bonding. According to the AIM analysis, the values of electron density and energy density at the M-O and M-N BCPs increase with the order of Eu(III) < U(VI) < Th(IV), which is indicative of the order of the bond strengths. The WBI and AIM results clearly demonstrate that the Et-Tol-DAPhen ligand favors actinides more than lanthanides, which is quite consistent with our previous results of solvent extraction[44].

Conclusions

To further elucidate the complexation of Et-Tol-DAPhen with actinides and lanthanides, the speciation of Eu(III), U(VI), and Th(IV) with Et-Tol-DAPhen in acetonitrile solution were investigated by using ESI-MS technique. The M-L complexes (M = Eu(III), U(VI), and Th(IV); L = Et-Tol-DAPhen) in ESI-MS spectra vary as a function of metal-to-ligand ratios. The MS peaks were dominated by 1:2 M-L species at low [M]/[L] ratios whereas the abundance of 1:1 M-L species increased with increasing metal-to-ligand ratio. However, regardless of the [M]/[L] ratios, only 1:1 U(VI) complex was observed in MS spectra. Nitrate-coordinated species are dominant and bare positive species, such as $[UO_2L]^{2+}$, $[EuL]^{3+}$ and $[ThL_2]^{4+}$, are not detected. CID reactions of all the M-L complexes showed that Et-Tol-DAPhen ligands can coordinate so strongly to the metal ions that only the side alkyl or aryl groups of amides in the ligands were eliminated from the complexes. The geometrical structure and bonding nature as well as thermodynamic stabilities of the M-L complexes were explored by DFT calculations. A higher degree of covalent character was found for the metal-ligand bonding in the actinide species. The predicted stable cationic M-L species in acetonitrile solution were consistent with the ESI-MS results. In fact, the results obtained in acetonitrile solution cannot be exactly the same as those obtained in real solvent extraction (Figs. S4-S6). Nevertheless, they provide quite similar data, which is beneficial to explore the complexation behaviour between metal ions and ligands.

This work was supported by the Major Research Plan "Breeding and Transmutation of Nuclear Fuel in Advanced Nuclear Fission Energy System" of the Natural Science Foundation of China (Grant Nos. 91326202) and the National Natural Science Foundation of China (Grant Nos. 11275219 and 21261140335), the "Strategic Priority Research Program" of the Chinese Academy of Sciences (Grant No. XDA030104), and the China Postdoctoral Science Foundation (Grant Nos. 2013M530734 and 2014T70123). This work is also supported by a project funded by the Priority Academic Program Development of Jiangsu Higher Education Institutions (PAPD). The results described in this work were obtained on the ScGrid of Supercomputing Center, Computer Network Information Center of Chinese Academy of Sciences.

Notes and references

[a] *School for Radiological and Interdisciplinary Sciences (RAD-X) and Collaborative Innovation Center of Radiation Medicine of Jiangsu Higher Education Institutions, Soochow University, Suzhou 215123, China. Tel: 86-512-65883945*

[b] *Laboratory of Nuclear Energy Chemistry and Key Laboratory For Biomedical Effects of Nanomaterials and Nanosafety, Institute of High Energy Physics, Chinese Academy of Sciences, Beijing 100049, China. Fax: 86-10-88235294; Tel: 86-10-88233968; E-mail: shiwq@ihep.ac.cn*

c Chemistry Department, Washington State University, Pullman 99164-4630, USA

† Electronic Supplementary Information (ESI) available: Experimental and simulated isotopic distribution of Eu(III), U(VI), and Th(IV) complexes with Et-Tol-DAPhen ligand (Figs. S1-S3), ESI-MS experiments after solvent extraction (Figs. S4-S6), all the ESI-MS data in tables (Tables S1-S4, S8, and S9), changes of the Gibbs free energy for forming acetonitrile complexes (Table S5), structure information of U(VI)-L complexes (Tables S6), and AIM analysis of $[UO_2L(NO_3)]^+$ (Table S7). See DOI: 10.1039/b000000x/

‡ These authors contributed equally to this work.

1. T. Inoue, M. Sakata, H. Miyashiro, T. Matsumura, A. Sasahara and N. Yoshiki, *Nucl Technol*, 1991, **93**, 206-220.
2. A. Salvatores, *Nucl Eng Des*, 2005, **235**, 805-816.
3. D. Warin, *J Nucl Sci Technol*, 2007, **44**, 410-414.
4. R. D. Shannon, *Acta Crystallogr A*, 1976, **32**, 751-767.
5. Z. Kolarik, *Chem Rev*, 2008, **108**, 4208-4252.
6. B. J. Mincher, G. Modolo and S. P. Mezyk, *Solvent Extr Ion Exch*, 2010, **28**, 415-436.
7. S. A. Ansari, P. Pathak, P. K. Mohapatra and V. K. Manchanda, *Sep Purif Rev*, 2011, **40**, 43-76.
8. B. J. Mincher, N. C. Schmitt and M. E. Case, *Solvent Extr Ion Exch*, 2011, **29**, 247-259.
9. M. Salvatores and G. Palmiotti, *Prog Part Nucl Phys*, 2011, **66**, 144-166.

10. Y. Q. Yang, S. Z. Luo, T. Z. Yang and F. H. Hao, *Prog Chem*, 2011, **23**, 1345-1354.
11. S. A. Ansari, P. Pathak, P. K. Mohapatra and V. K. Manchanda, *Chem Rev*, 2012, **112**, 1751-1772.
12. J. C. Braley, T. S. Grimes and K. L. Nash, *Ind Eng Chem Res*, 2012, **51**, 629-638.
13. G. Modolo, A. Wilden, A. Geist, D. Magnusson and R. Malmbeck, *Radiochim Acta*, 2012, **100**, 715-725.
14. M. J. Hudson, L. M. Harwood, D. M. Laventine and F. W. Lewis, *Inorg Chem*, 2013, **52**, 3414-3428.
15. J. H. Lan, W. Q. Shi, L. Y. Yuan, J. Li, Y. L. Zhao and Z. F. Chai, *Coord Chem Rev*, 2012, **256**, 1406-1417.
16. J. R. Klaehn, D. R. Peterman, M. K. Harrup, R. D. Tillotson, T. A. Luther, J. D. Law and L. M. Daniels, *Inorg Chim Acta*, 2008, **361**, 2522-2532.
17. Y. J. Zhu, J. F. Chen and G. R. Choppin, *Solvent Extr Ion Exch*, 1996, **14**, 543-553.
18. Y. J. Zhu, J. Chen and R. Z. Jiao, *Solvent Extr Ion Exch*, 1996, **14**, 61-68.
19. J. Chen, Y. J. Zhu and R. Z. Jiao, *Sep Sci Technol*, 1996, **31**, 2723-2731.
20. A. Geist, U. Mullich, D. Magnusson, P. Kaden, G. Modolo, A. Wilden and T. Zevaco, *Solvent Extr Ion Exch*, 2012, **30**, 433-444.
21. S. Trumm, A. Geist, P. J. Panak and T. Fanghanel, *Solvent Extr Ion Exch*, 2011, **29**, 213-229.
22. Z. Kolarik, U. Mullich and F. Gassner, *Solvent Extr Ion Exch*, 1999, **17**, 23-32.
23. Z. Kolarik, U. Mullich and F. Gassner, *Solvent Extr Ion Exch*, 1999, **17**, 1155-1170.
24. J. Narbutt and W. P. Oziminski, *Dalton Trans*, 2012, **41**, 14416-14424.
25. F. W. Lewis, L. M. Harwood and V. P. Krasnov, *Eur J Org Chem*, 2012.
26. J. H. Lan, W. Q. Shi, L. Y. Yuan, Y. X. Feng, Y. L. Zhao and Z. F. Chai, *J Phys Chem A*, 2012, **116**, 504-511.
27. J. H. Lan, W. Q. Shi, L. Y. Yuan, Y. L. Zhao, J. Li and Z. F. Chai, *Inorg Chem*, 2011, **50**, 9230-9237.
28. V. Hubscher-Bruder, J. Haddaoui, S. Bouhroum and F. Arnaud-Neu, *Inorg Chem*, 2010, **49**, 1363-1371.
29. M. R. S. Foreman, M. J. Hudson, M. G. B. Drew, C. Hill and C. Madic, *Dalton Trans*, 2006, 1645-1653.
30. F. W. Lewis, L. M. Harwood, M. J. Hudson, M. G. Drew, V. Hubscher-Bruder, V. Videva, F. Arnaud-Neu, K. Stamberg and S. Vyas, *Inorg Chem*, 2013.
31. A. Afsar, D. M. Laventine, L. M. Harwood, M. J. Hudson and A. Geist, *Chem Commun*, 2013, **49**, 8534-8536.
32. F. W. Lewis, L. M. Harwood, M. J. Hudson, M. G. B. Drew, A. Wilden, M. Sypula, G. Modolo, T.-H. Vu, J.-P. Simonin, G. Vidick, N. Bouslimani and J. F. Desreux, *Procedia Chem*, 2012, **7**, 231-238.
33. F. W. Lewis, M. J. Hudson and L. M. Harwood, *Synlett*, 2011, 2609-2632.
34. F. W. Lewis, L. M. Harwood, M. J. Hudson, M. G. B. Drew, J. F. Desreux, G. Vidick, N. Bouslimani, G. Modolo, A. Wilden, M. Sypula, T. H. Vu and J. P. Simonin, *J Am Chem Soc*, 2011, **133**, 13093-13102.
35. K. Bell, C. Carpentier, M. Carrott, A. Geist, C. Gregson, X. Heres, D. Magnusson, R. Malmbeck, F. McLachlan, G. Modolo, U. Mullich, M. Sypula, R. Taylor and A. Wilden, *Procedia Chem*, 2012, **7**, 392-397.
36. E. Aneheim, C. Ekberg, M. R. S. Foreman, E. Lofstrom-Engdahl and N. Mabile, *Sep Sci Technol*, 2012, **47**, 663-669.
37. E. Aneheim, C. Ekberg, A. Fermvik, M. R. S. J. Foreman, B. Gruner, Z. Hajkova and M. Kvicalova, *Solvent Extr Ion Exch*, 2011, **29**, 157-175.
38. E. Aneheim, C. Ekberg, A. Fermvik, M. R. S. Foreman, T. Retegan and G. Skarnemark, *Solvent Extr Ion Exc*, 2010, **28**, 437-458.
39. E. Aneheim, C. Ekberg, A. Fermvik and M. R. S. Foreman, *Nuclear Energy and the Environment*, 2010, **1046**, 119-130.
40. C. Marie, M. Miguirditchian, D. Guillaumont, A. Tosseng, C. Berthon, P. Guilbaud, M. Duvail, J. Bisson, D. Guillaneux, M. Pipelier and D. Dubreuil, *Inorg Chem*, 2011, **50**, 6557-6566.
41. C. Marie, M. Miguirditchian, D. Guillaneux, J. Bisson, M. Pipelier and D. Dubreuil, *Solvent Extr Ion Exch*, 2011, **29**, 292-315.
42. T. Kobayashi, T. Yaita, S. Suzuki, H. Shiwaku, Y. Okamoto, K. Akutsu, Y. Nakano and Y. Fujii, *Sep Sci Technol*, 2010, **45**, 2431-2436.
43. J. Bisson, C. Berthon, L. Berthon, N. Boubals, D. Dubreuil and M. C. Charbonnel, *Procedia Chem*, 2012, **7**, 13-19.
44. C. L. Xiao, C. Z. Wang, L. Y. Yuan, B. Li, H. He, S. Wang, Y. L. Zhao, Z. F. Chai and W. Q. Shi, *Inorg Chem*, 2014, **53**, 1712-1720.
45. L. W. McDonald, J. A. Campbell and S. B. Clark, *Anal Chem*, 2014, **86**, 1023-1029.
46. S. Colette, B. Amekraz, C. Madic, L. Berthon, G. Cote and C. Moulin, *Inorg Chem*, 2002, **41**, 7031-7041.
47. S. Colette, B. Amekraz, C. Madic, L. Berthon, G. Cote and C. Moulin, *Inorg Chem*, 2003, **42**, 2215-2226.
48. Y. Gong, H. S. Hu, L. F. Rao, J. Li and J. K. Gibson, *J Phys Chem A*, 2013, **117**, 10544-10550.
49. Y. Gong, H. S. Hu, G. X. Tian, L. F. Rao, J. Li and J. K. Gibson, *Angew Chem Int Edit*, 2013, **52**, 6885-6888.
50. Y. Gong, G. X. Tian, L. F. Rao and J. K. Gibson, *J Phys Chem A*, 2014, **118**, 2749-2755.
51. T. Retegan, L. Berthon, C. Ekberg, A. Fermvik, G. Skarnemark and N. Zorz, *Solvent Extr Ion Exch*, 2009, **27**, 663-682.
52. M. J. Frisch, G. W. Trucks, H. B. Schlegel, G. E. Scuseria, M. A. Robb, J. R. Cheeseman, G. Scalmani, V. Barone, B. Mennucci, G. A. Petersson, H. Nakatsuji, M. Caricato, X. Li, H. P. Hratchian, A. F. Izmaylov, J. Bloino, G. Zheng, J. L. Sonnenberg, M. Hada, M. Ehara, K. Toyota, R. Fukuda, J. Hasegawa, M. Ishida, T. Nakajima, Y. Honda, O. Kitao, H. Nakai, T. Vreven, J. A. Montgomery, Jr., J. E. Peralta, F. Ogliaro, M. Bearpark, J. J. Heyd, E. Brothers, K. N. Kudin, V. N. Staroverov, R. Kobayashi, J. Normand, K. Raghavachari, A. Rendell, J. C. Burant, S. S. Iyengar, J. Tomasi, M. Cossi, N. Rega, J. M. Millam, M. Klene, J. E. Knox, J. B. Cross, V. Bakken, C. Adamo, J. Jaramillo, R. Gomperts, R. E. Stratmann, O. Yazyev, A. J. Austin, R. Cammi, C. Pomelli, J. W. Ochterski, R. L. Martin, K. Morokuma, V. G. Zakrzewski, G. A. Voth, P. Salvador, J. J. Dannenberg, S. Dapprich, A. D. Daniels, Ö. Farkas, J. B. Foresman, J. V. Ortiz, J. Cioslowski and D. J. Fox, Gaussian 09, Revision A.1, Gaussian, Inc., Wallingford CT, 2009.
53. A. D. Becke, *Phys Rev A*, 1988, **38**, 3098-3100.
54. C. T. Lee, W. T. Yang and R. G. Parr, *Phys Rev B*, 1988, **37**, 785-789.
55. W. Kuchle, M. Dolg, H. Stoll and H. Preuss, *J Chem Phys*, 1994, **100**, 7535-7542.
56. M. Dolg, H. Stoll and H. Preuss, *J Chem Phys*, 1989, **90**, 1730-1734.
57. A. Klamt and G. Schuurmann, *J Chem Soc Perk T 2*, 1993, 799-805.
58. M. Cossi, N. Rega, G. Scalmani and V. Barone, *J Comput Chem*, 2003, **24**, 669-681.
59. V. Barone and M. Cossi, *J Phys Chem A*, 1998, **102**, 1995-2001.
60. J. Andzelm, C. Kolmel and A. Klamt, *J Chem Phys*, 1995, **103**, 9312-9320.
61. K. B. Wiberg, *Tetrahedron*, 1968, **24**, 1083-1096.
62. T. Lu and F. W. Chen, *J Comput Chem*, 2012, **33**, 580-592.
63. C. L. Xiao, Q. Y. Wu, C. Z. Wang, Y. L. Zhao, Z. F. Chai and W. Q. Shi, *Sci China Chem*, 2014, **57**, 1439-1448.
64. C. L. Xiao, Q. Y. Wu, C. Z. Wang, Y. L. Zhao, Z. F. Chai and W. Q. Shi, *Inorg Chem*, 2014, **53**, 10846-10853.
65. A. Savin, O. Jepsen, J. Flad, O. K. Andersen, H. Preuss and H. G. Vonschnering, *Angew Chem Int Edit*, 1992, **31**, 187-188.
66. L. Petit, L. Joubert, P. Maldivi and C. Adamo, *J Am Chem Soc*, 2006, **128**, 2190-2191.
67. E. Di Santo, M. D. Michelini and N. Russo, *Organometallics*, 2009, **28**, 3716-3726.
68. K. E. Laidig and R. F. W. Bader, *J Chem Phys*, 1990, **93**, 7213-7224.
69. A. D. Becke, *J Chem Phys*, 2013, **138**.